J. Fluid Mech. (2007), *vol.* 588, *pp.* 331–351.
doi:10.1017/S0022112007007574 Printed in the United Kingdom

Two alternatives for solving hyperbolic boundary value problems of geophysical fluid dynamics

UWE HARLANDER† AND LEO R. M. MAAS

Royal Netherlands Institute for Sea Research, P.O. Box 59, 1790AB, Texel, The Netherlands

(Received 8 June 2006 and in revised form 18 May 2007)

Linear internal waves in inviscid bounded fluids generally give a mathematically ill-posed problem since hyperbolic equations are combined with elliptic boundary conditions. Such problems are difficult to solve. Two new approaches are added to the existing methods: the first solves the two-dimensional spatial wave equation by iteratively adjusting Cauchy data such that boundary conditions are satisfied along a predefined boundary. After specifying the data in this way, solutions can be computed using the d'Alembert formula.

The second new approach can numerically solve a wider class of two dimensional linear hyperbolic boundary value problems by using a 'boundary collocation' technique. This method gives solutions in the form of a partial sum of analytic functions that are, from a practical point of view, more easy to handle than solutions obtained from characteristics. Collocation points have to be prescribed along certain segments of the boundary but also in the so-called fundamental intervals, regions along the boundary where Cauchy data can be given arbitrarily without over- or under-determining the problem. Three prototypical hyperbolic boundary value problems are solved with this method: the Poincaré, the Telegraph, and the Tricomi boundary value problem. All solutions show boundary-detached internal shear layers, typical for hyperbolic boundary value problems. For the Tricomi problem it is found that the matrix that has to be inverted to find solutions from the collocation approach is ill-conditioned; thus solutions depend on the distribution of the collocation points and need to be regularized.

1. Introduction

It is well known that a particular type of linear second-order partial differential equation (PDE) can be combined only with a particular type of boundary condition (BC) to give a well-posed boundary value problem (BVP) (Morse & Feshbach 1953, p. 706). (A general definition of well-posed is given in Payne (1975). Here it implies that a unique solution exists that changes continuously with the boundary geometry.) For problems with a fully closed boundary, for instance, only elliptic PDEs with Dirichlet or von Neumann BCs are well-posed. Nevertheless, many relevant BVPs of mathematical physics in general and geophysical fluid dynamics (GFD) in particular are governed by linear second order hyperbolic equations in closed domains and hence are ill-posed. Consider for example an inviscid fluid comprised between two co-rotating spheres (Stewartson & Rickard 1969; Brown & Stewartson 1976). In GFD

† Present address: Department of Aerodynamics and Fluid Mechanics, Brandenburg University of Technology (BTU) Cottbus, Siemens-Halske-Ring 14, 03046 Cottbus, Germany.

it is important to understand the free periods of oscillation of this BVP, which might help to understand the motion in the Earth's fluid outer core, and the Earth's oceans or its atmosphere (when the tropopause is seen as a wave reflector). Nevertheless, this problem is ill-posed since a hyperbolic PDE has to be combined with Dirichlet BCs.

Some explicit solutions of hyperbolic BVPs have been found for particular geometries, for example a cylinder (Kelvin 1880) or a full elipsoid (Bryan 1889), all being continuously differentiable (smooth) functions. In general, however, a typical feature of hyperbolic BVPs is the occurrence of singularities (Stewartson & Rickard 1969; Rieutord, Georgeot & Valdettaro 2000; Maas 2005).

The situation is summarized in the apposite remark by Professor A. Seeger in the preface to Slavyanov & Lay (2000): 'The mathematical description of physical problems always requires simplifications, and those often introduce *singularities*. The essentials of a physical problem are, in fact, usually contained in the location and character of the singularities. However, numerical handling of singularities, be they in the equations or in the solutions, is always a delicate matter, for which still no general recipe is available.' In the GFD context, the simplifications leading to singularities are the neglect of nonlinearity and viscosity. The essentials of a hyperbolic BVP appear to be contained in the web of characteristics† and its limit cycle, called the wave attractor (Maas & Lam 1995) on which the velocity field becomes singular. And, indeed, there is no general recipe for handling hyperbolic BVPs.

A method that maps characteristics into certain boundary regions (called fundamental intervals) to find, at discrete points, exact solutions of the two-dimensional Poincaré BVP was developed by Maas & Lam (1995). This Poincaré BVP is written $\psi_{yy} - \psi_{zz} = 0$, with $\psi = 0$ along the boundary, where $\psi(y, z)$ is the dependent variable, and y, z are the independent variables. Cauchy data, containing directional derivatives in the direction normal to the boundary, are given in the fundamental intervals only, where they can be prescribed arbitrarily without over-or under-determining the problem. The disadvantage of the Maas & Lam approach is that it works only for the two-dimensional Poincaré equation and a generalization to other equations seems to be impossible.

To attack hyperbolic BVPs numerically, singularities have to be *regularized* to find meaningful approximate solutions. Several authors have used small viscosity for regularization (Hollerbach & Kerswell 1995; Rieutord, Georgeot & Valdettaro 2001; Ogilvie & Lin 2004). Recently, Swart *et al.* (2007) used a minimal-energy regularization to numerically solve the two-dimensional Poincaré equation. In contrast to the methods of Maas & Lam (1995) and Swart *et al.* (2007), the small-viscosity method can be applied to a larger class of hyperbolic BVPs. However, as pointed out by Swart *et al.* (2007), for very small viscosity the existence of many nearby eigenvalues makes it difficult to find all solutions on a finite grid so that the problem remains ill-posed from a numerical point of view.

In the present paper we will add two alternatives to the methods above. The first solves the two-dimensional Poincaré equation as a well-posed Cauchy problem, perturbing the boundary data iteratively. In contrast to Maas & Lam (1995), no knowledge about fundamental intervals is necessary; in contrast to Swart *et al.* (2007) no regularization is necessary. However, the method works only when we can start the iteration with a geometry for which the Poincaré BVP possesses smooth solutions that can be found by using separation of variables. In this sense the method is less

† A second-order hyperbolic PDE has two families of real characteristics. Following a characteristic and switching from one family to the other at boundary reflections yields a web of characteristics that converges towards a limit cycle.

flexible than the method of Maas & Lam (1995) or Swart *et al.* (2007). The second method proposed here superposes exact smooth solutions of a separable and solvable hyperbolic BVP to construct approximate solutions in a perturbed domain. In contrast to the three methods mentioned above, this 'boundary collocation' technique can be applied to more general hyperbolic BVPs. The method appears to be simpler than numerical low-viscosity methods. However, it is less flexible in the sense that it cannot be applied to arbitrary geometries.

By use of the boundary collocation technique, we try to answer the question of whether wave attractors play a similar role for non-separable BVPs† as for the two-dimensional Poincaré problem, the archetype of a separable BVP. For non-separable problems, characteristics can generally not be used to construct solutions. The question is whether wave attractors of non-separable equations still contain the essentials of the problem, that is singularities and, adding viscosity, local regions of strong dissipation. For slightly viscous problems, this question has already been addressed by comparing localized eigenfunctions with corresponding non-viscous wave attractors (Dintrans, Rieutord & Valdettaro 1999; Rieutord *et al.* 2001). We investigate this question by studying the Telegraph equation $\psi_{yy} - \psi_{zz} + \alpha^2\psi = 0$ (with α^2 constant) and the Tricomi equation $\psi_{yy} + y\psi_{zz} = 0$ for geometries corresponding to a simple wave attractor. In addition, in Appendix B, we estimate the rate of dissipation from the spectral coefficients of the series solutions of the two-dimensional Poincaré problem.

The Telegraph equation forms a model for time-harmonic small-amplitude internal gravity waves in a strongly stratified fluid. The Tricomi equation is archetypal for problems that are hyperbolic in some part of the domain of interest but elliptic elsewhere. Such mixed problems are important in GFD (Friedlander 1982; Friedlander & Siegmann 1982; Dintrans *et al.* 1999), for example in the context of trapped equatorial waves (Maas & Harlander 2007). Such waves can propagate in the hyperbolic region but are trapped between turning surfaces. Beyond those surfaces the equation is elliptic and wave propagation is not possible.

The paper is organized as follows. In § 2 we give some physical motivation for the equations considered. In § 3 we describe the iterative technique by solving the two-dimensional Poincaré BVP. We consider an almost rectangular confinement but with sloping parts at the bottom. In § 4 we explain the boundary collocation method by considering three BVPs: the two-dimensional Poincaré, the Telegraph, and the Tricomi BVP for half-trapezoidal regions. Finally, in § 5 we give a brief summary and conclusions.

2. Physical motivation

In the following we derive three 'prototypical' equations from the Boussinesq equations. Together with appropriate boundary conditions, these three equations form the hyperbolic boundary value problems that will be solved later.

The zonally symmetric ($\partial/\partial x = 0$) Boussinesq equations for a rotating fluid are, in a Cartesian frame (y, z),

$$u_t - fv = 0, \tag{2.1}$$

† Here the separability of the equation's operator is meant. If $\mathscr{L}\psi = 0$ (where $\mathscr{L}$ is a linear second-order operator) can be written as $\mathscr{P}_1\mathscr{P}_2\psi = 0$ with two first-order linear operators $\mathscr{P}_i = a_i(y,z)\partial/\partial y + b_i(y,z)\partial/\partial z$, $i = 1, 2$, then $\mathscr{L}$ is called separable. Introducing new coordinates such that $\partial_\eta = \mathscr{P}_1$ and $\partial_\zeta = \mathscr{P}_2$ (with $\eta_z\zeta_y - \eta_y\zeta_z \neq 0$), the PDE can be written as $\psi_{\eta\zeta} = 0$, thus is solvable for any closed domain (Maas & Lam 1995).

$$v_t + fu + p_y/\rho_0 = 0, \tag{2.2}$$

$$w_t + p_z/\rho_0 + g\rho/\rho_0 = 0, \tag{2.3}$$

$$\rho_t - (N^2\rho_0/g)w = 0, \tag{2.4}$$

$$v_y + w_z = 0, \tag{2.5}$$

where t is time, $\boldsymbol{v} = (u, v, w)$ is the velocity vector, p perturbation pressure, ρ perturbation density, $\rho_0(z)$ the background density, $N^2 = -g\rho_{0_z}/\rho_0$ the buoyancy frequency squared, f the Coriolis parameter, and g is the acceleration due to gravity. Subscripts t, y, z denote partial derivatives. We restrict consideration to uniformly stratified fluids where N is constant. This system of equations can be reduced to a single equation in w. For $f = 0$ we obtain

$$\nabla^2 w_{tt} + 2\alpha\, w_{ttz} + N^2 w_{yy} = 0, \tag{2.6}$$

with $\nabla = (\partial/\partial y, \partial/\partial z)$ and $\alpha = -N^2/2g$.

Because of zonal symmetry we can introduce a streamfunction $v = -\psi_z$ and $w = \psi_y$. Using $\psi = \hat{\psi}(y, z)\exp(\alpha z - \mathrm{i}\omega t)$, where ω is the wave's frequency, and $\mathrm{i} = (-1)^{1/2}$, and defining $y = ((N^2 - \omega^2)/\omega^2)^{1/2}\tilde{y}$, we obtain

$$\hat{\psi}_{\tilde{y}\tilde{y}} - \hat{\psi}_{zz} + \alpha^2\hat{\psi} = 0. \tag{2.7}$$

This is the *Telegraph equation*. Boundary conditions are $\hat{\psi} = 0$ at the boundary.

Frequently, it is assumed that α is small and the second term of (2.6) is neglected. Then (2.7) reduces to the *two-dimensional Poincaré equation*

$$\hat{\psi}_{\tilde{y}\tilde{y}} - \hat{\psi}_{zz} = 0, \tag{2.8}$$

with $\hat{\psi} = 0$ at the boundary.

Finally, replacing $\rho_0(z)$ by a constant $\bar{\rho}$ in (2.1) to (2.4) and in the denominator of N^2, we consider the hydrostatic, zonally symmetric Boussinesq version of (2.1) to (2.5) for an equatorial β-plane, where $f = \beta y$ with β constant. Considering time-harmonic solutions and introducing a streamfunction in the meridional plane we obtain

$$\psi_{yy} - \frac{\omega^2 - \beta^2 y^2}{N^2}\psi_{zz} = 0. \tag{2.9}$$

This equation changes type across two turning curves where $y = \pm\omega/\beta$. Enlarging one turning curve by introducing $\beta y = \omega + \epsilon\tilde{y}$, defining $z = (2\epsilon^3\omega)^{1/2}\tilde{z}/(\beta N)$ and neglecting the order- ϵ term, we find

$$\psi_{\tilde{y}\tilde{y}} + \tilde{y}\psi_{\tilde{z}\tilde{z}} = 0. \tag{2.10}$$

This is the *Tricomi equation*, which forms the prototypical mixed problem, hyperbolic for $\tilde{y} < 0$ and elliptic for $\tilde{y} \geqslant 0$ with a turning curve at $\tilde{y} = 0$. Boundary condition is $\psi = 0$ along the boundary.

3. Solving Poincaré's BVP as a Cauchy problem

As stated above, the problem of finding solutions of the two-dimensional Poincaré BVP

$$\psi_{yy} - \psi_{zz} = 0, \quad \text{with} \quad \psi = 0 \quad \text{at} \quad \partial M, \tag{3.1}$$

where M denotes the domain of interest and ∂M the closed boundary thereof, has already been solved by Maas & Lam (1995). However, it is worth tackling this

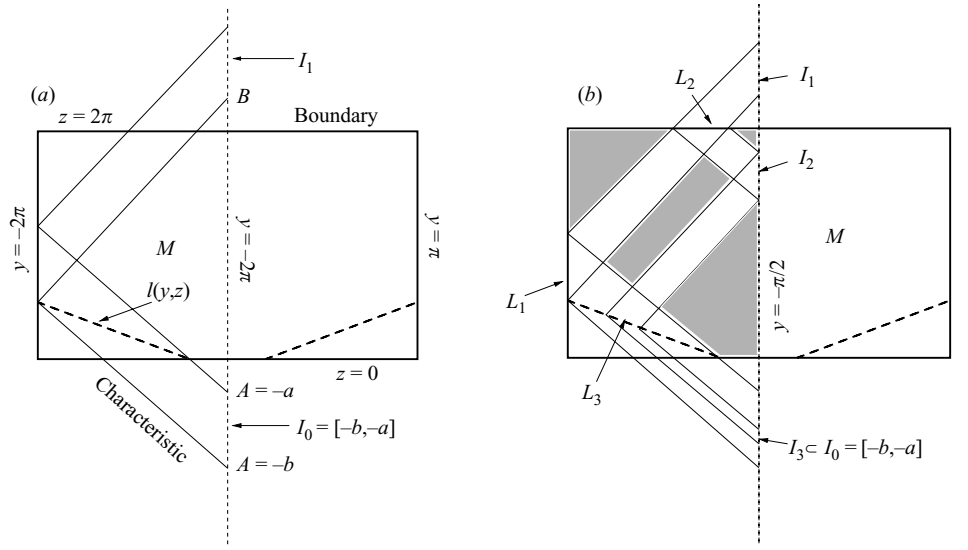

FIGURE 1. Rectangular domain M (bold solid lines) and perturbations (shown by dashed lines). Thin solid lines show characteristics. Data are given along $y = -\pi/2$. The intervals I_j, $j = 0, \ldots, 3$ and L_j, $j = 1, 2, 3$ are defined by characteristics. The intervals I_j are situated on the data curve, the intervals L_j along the boundary. For more details see the text.

problem from a different perspective. Maas & Lam focused on the possibility of transforming an ill-posed problem to a well-posed one by reducing the amount of data along the boundary. Here we consider the problem as a well-posed Cauchy problem and try to control the boundary by perturbing the Cauchy data iteratively. The major advantage of this approach is that it does not depend on knowledge of fundamental intervals. Note that neither the method by Maas & Lam (1995) nor the method proposed here needs regularization. Moreover, both methods can easily handle non-smooth solutions.

Step one

Let us start with a certain $\psi = \psi_0(y, z)$ that solves (3.1) in the rectangle. Such solutions can be found by separation of variables as long as the width L_y and the height L_z of the rectangle are commensurable, that is $L_y/L_z = q$, where q is a rational number. We consider a rectangle given by $z = 0, 2\pi$, $y = -2\pi, \pi$ (see the bold solid lines in figure 1*a*). We take $f(z) = \psi_0(-\pi/2, z)$ and $g(z) = \psi_y(-\pi/2, z)$ as (Cauchy) data along the curve $y = -\pi/2$. Note that it is not necessary to define $f(z)$ and $g(z)$ for all z. However, it is not sufficient to define $f(z)$ and $g(z)$ just for the interval $z \in [0, 2\pi]$. In fact, the upper boundary of z is given by the upward-sloping characteristic connecting the data curve with the upper left corner $(y, z) = (-2\pi, 2\pi)$ of the rectangle, and the lower boundary of z is given by the downward-sloping characteristic connecting the data curve with the lower left corner $(y, z) = (-2\pi, 0)$ (see figure 1*a*).

Since $y = -\pi/2$ is a line of symmetry, we assume without loss of generality that $g(z) = 0$. As is discussed in Appendix A, at any point P within the domain M, the streamfunction ψ is given by

$$\psi_P = \tfrac{1}{2}((\psi)\,|_A + (\psi)\,|_B), \tag{3.2}$$

which is d'Alembert's formula. A and B are the intersections of the characteristic curves through P with the curve $y = -\pi/2$ (see Appendix A and figure 7*a*). Note that owing to the symmetry it is sufficient to consider the solution in the region to the left of the axis $y = -\pi/2$. Let us introduce a 'perturbation' of the boundary at the lower left and lower right corner of M (shown as dashed lines in figure 1). In other words, we introduce a new zero level set $\{(y, z) \in M : \psi(y, z) = 0\} \in \mathbb{R}^2$ of the solution in M. This curve, denoted by l, is given as

$$z = -(sy + r), \tag{3.3}$$

where s and r are constants. From the boundary conditions in (3.1) we know that

$$(\psi)\,|_A = -(\psi)\,|_B \tag{3.4}$$

along l. This condition enables us to compute the new data in the interval $I_0 = [-b, -a]$ (see figure 1*a*), where $a = \pi/2 - r/s$ and $b = 2\pi s - r - 3\pi/2$. Using the equations for the c^+- and c^--characteristics $z \mp y = c^{\pm}$ we can relate A and B to the coordinates y, z of P (see figure 7*a*):

$$A = z + y + \tfrac{1}{2}\pi, \tag{3.5}$$

$$B = z - y - \tfrac{1}{2}\pi. \tag{3.6}$$

Along l we therefore obtain

$$A = \frac{z(s-1) - r + \frac{1}{2}\pi s}{s} \tag{3.7}$$

$$B = \frac{z(s+1) + r - \frac{1}{2}\pi s}{s}, \tag{3.8}$$

or

$$z(A) = \frac{As + r - \frac{1}{2}\pi s}{s-1} \tag{3.9}$$

$$z(B) = \frac{Bs - r + \frac{1}{2}\pi s}{s+1}. \tag{3.10}$$

Finally, from (3.4) we find that in I_0

$$f_{I_0}(A) = -f_{I_1}(B) = -f\left(\frac{z(A)(s+1) + r - \frac{1}{2}\pi s}{s}\right), \tag{3.11}$$

to satisfy the boundary condition along l. The interval I_1 corresponding to I_0 is shown in figure 1*a*.

Step two

In processing the first step we introduced a new zero level set of ψ along l. Unfortunately, this operation removes the zeros along the boundary in the interval L_1, shown in figure 1*b*. To correct this, we introduce new data in the interval I_1 by using a similar approach to the one described in detail for step one. From (3.4) we find that in I_1

$$f_{I_1}(B) = -f(B - 3\pi), \tag{3.12}$$

to satisfy the boundary conditions in L_1.

Step three

The correction done for I_1 removes the zeros along the upper boundary in L_2. This can be corrected by introducing new data in the interval I_2. From (3.4) we find that in I_2

$$f_{I_2}(A) = -f(4\pi - A), \tag{3.13}$$

to satisfy the boundary conditions in L_2. As is obvious from figure 1(*b*), this affects the zero level in a small piece of l, denoted by L_3. We can state that as long as characteristic focusing is present, $I_3 \subset I_0$.

Summary of the three steps

Let us briefly summarize the three steps above. The goal of the iteration described is to modify the data $f(z)$ along $y = -\pi/2$ such that the BVP (3.1) is no longer satisfied for the rectangle but is fulfilled approximately for the trapezium. In step one we modified $f(z)$ in the interval I_0 (see figure 1*a*) such that $\psi = 0$ along the sloping part of the boundary. Unfortunately, the new data in I_0 gave a ψ that did not satisfy the boundary condition in the interval L_1 (see figure 1*b*). Therefore we needed step two in which we modified $f(z)$ in the interval I_1 such that $\psi = 0$ along the boundary interval L_1. Again, the new data in I_1 gave a ψ that did not satisfy the boundary condition in the interval L_2. Thus, we needed a third step in which we modified $f(z)$ in the interval I_2 such that $\psi = 0$ along the boundary interval L_2. After step three we obtained a ψ that satisfied the boundary condition everywhere, except in small part of the sloping boundary, L_3.

The first cycle of iteration is now complete and we obtain an order-one approximation of the solution in the deformed domain. To obtain an order-n approximation, we have to repeat step one to three n times.

Note that in some parts of the domain, the original analytical solution for the rectangular domain remains intact even when a sloping sidewall is introduced. Such 'shadow zones' (Rieutord *et al.* 2001) are shaded in figure 1*b*. Note further that the accuracy of the solution depends on the focusing rate. The stronger the focusing, the better is the approximation after n iterations. The focusing rate γ is given by the ratio of the length of I_0, denoted by $\bar{I}_0$, and the length of I_3, $\bar{I}_3$. More generally, $\gamma = \bar{I}_{k+3}/\bar{I}_k$, for all $k = 0, 1, 2, \ldots$. The focusing rate can most easily be found by using the two c^+-characteristics, one through the starting point of the slope $(y, z) = (-r/s, 0)$ and one through its endpoint $(y, z) = (-2\pi, 2\pi s - r)$, to compute an interval along the axis $y = -\pi/2$ and compare this with the interval I_0. We find

$$\gamma = \frac{1 - s}{1 + s}. \tag{3.14}$$

For $s = 0$ there is no focusing ($\gamma = 1$) and smooth solutions can be found. For $s \in]0, 1[$, we obtain focusing; for $s \in]1, \infty[$, γ is negative, i.e. we find defocusing. Note that for the defocusing case also attractors can exist, but then for waves travelling in the counterclockwise direction. For the critical slope $s = 1$, focusing becomes infinitely large ($1/\gamma = \infty$) and singularities can be expected along the slope. After n iterations, the length of the subinterval in I_0 (denoted by $\bar{I}_{3n}$, see figure 1*b*), is given by

$$\bar{I}_{3n} = \gamma^n \bar{I}_0. \tag{3.15}$$

In figure 2 we show an example. We used $f = -\sin z$, $r = 5.4/(2\pi - 2.7)$, and $s = r/2.7$. This choice of parameters corresponds to a significant focusing with $\gamma \approx 0.28$. Figure 2(*a*) shows ψ_0, the solution for the rectangle (solid bold lines in

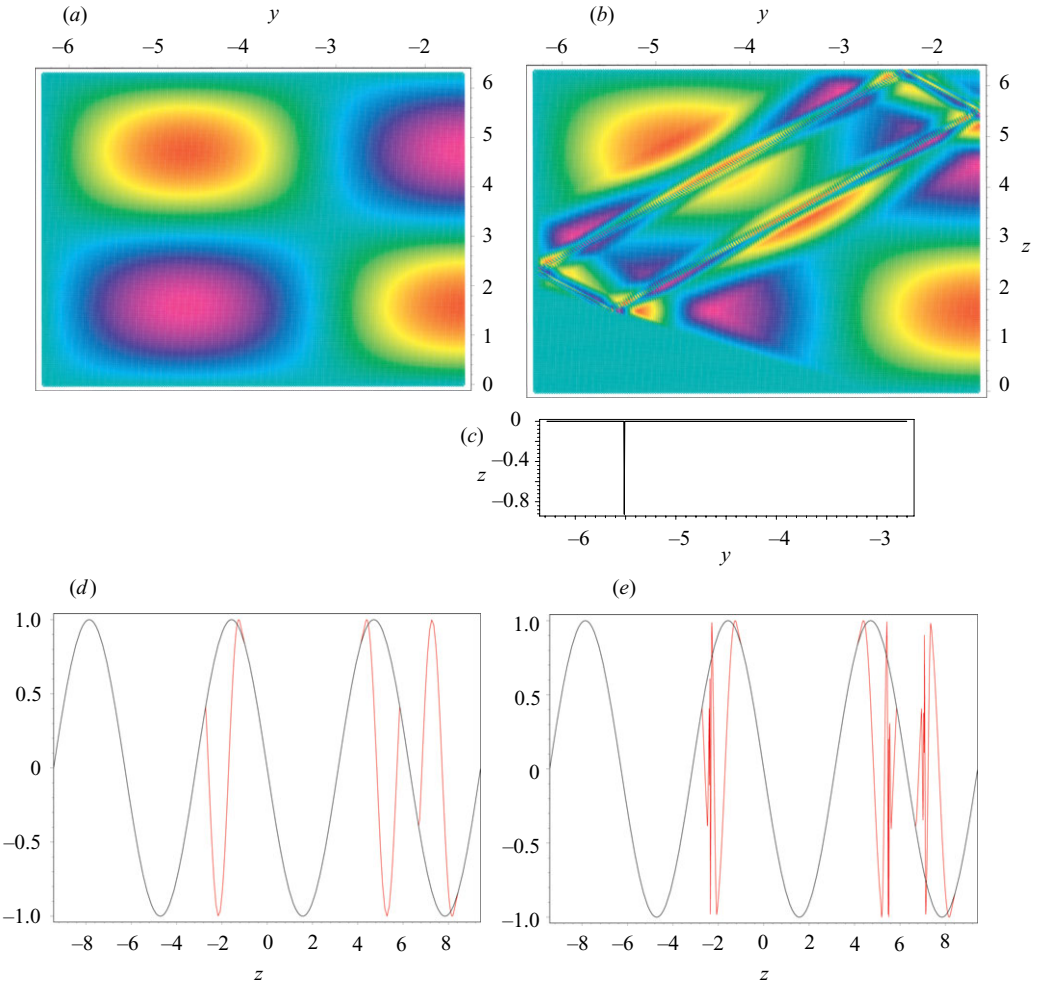

FIGURE 2. Solution ψ corresponding to $f(z) = -\sin z$. (*a*) Solution for the rectangle shown in figure 1 (bold solid lines). (*b*) Solution ψ for the deformed rectangle with $r = 5.4/(2\pi - 2.7)$, and $s = r/2.7$ after five iteration cycles ($n = 5$). (*c*) ψ along the slope l and plotted versus y. (*d*) Initial data $f(z)$ along $y = -\pi/2$ (black line), data after one iteration cycle ($n = 1$) (red line). (*e*) Initial data $f(z)$ along $y = -\pi/2$ (black line), data after five iteration cycles ($n = 5$) (red line).

figure 1). It was computed by applying (3.2) for a large set of points in M. Next the boundary is deformed as indicated by the dashed lines in figure 1. The fifth-order approximation is displayed in figure 2(*b*). The wave attractor is clearly visible as an internal boundary layer with large gradients. Figure 2(*c*) shows ψ when plotted along the sloping boundary. Obviously, the boundary condition is violated in a small neighbourhood of the point where the wave attractor is reflected from the slope. From (3.15) we find that the width of this region is of order 10^{-3} for $n = 5$, converging rapidly to zero for $n \to \infty$. Figure 2(*d*) shows $f(z)$, $z \in [-3\pi, 3\pi]$ for $n = 0$ (black curve) and $n = 1$ (red curve), figure 2(*e*) shows $f(z)$ for $n = 0$ and $n = 5$. It can be seen that three regions with large $\mathrm{d}f/\mathrm{d}z$ develop. For $n \to \infty$, singularities would arise in these regions. Note that only one of the three singularities of $\mathrm{d}f/\mathrm{d}z$ is located in M. The other two are outside the domain of interest and correspond to the

Boundary	c^-	c^+
slope	$f\left(\dfrac{z(A)(s+1)+r-\frac{1}{2}\pi s}{s}\right)$	$f\left(\dfrac{z(B)(s-1)-r+\frac{1}{2}\pi s}{s}\right)$
left	$f(A+3\pi)$	$f(B-3\pi)$
upper	$f(4\pi-A)$	$f(4\pi-B)$
lower	$f(-A)$	$f(-B)$

TABLE 1. Correction formulae for all boundaries. Note that A and B are located in two different intervals along $y=-\pi/2$. For A, the interval is determined by two c^--characteristics, for B by two c^+-characteristics.

extension of the two branches of the attractor that are not connected with $y=-\pi/2$ (see figure 2(b)). It is obvious that Cauchy data have to be given outside M also in order to find a solution in the closed domain M. Note that the solution shown in figure 2(b) is usually stable with respect to small changes of the slope. However, at certain slopes, the wave attractor, and thus the solution, changes its shape suddenly. This behaviour is discussed in more detail by Maas & Harlander (2007).

In summary we give the 'correction formulae' for each boundary with respect to c^-- and c^+-characteristics in table 1. Note that intersections of a c^--characteristic with the curve $y=-\pi/2$ are denoted by A, and intersections of a c^+-characteristic are denoted by B. The table should be read in the following way: if the left boundary has to be corrected by changing data in an interval given by two c^--characteristics, then use $f_l(A)=f(A+3\pi)$ and so forth.

4. Solving hyperbolic BVPs approximately by a boundary collocation method

In this section we discuss an alternative approach to solve hyperbolic BVPs. Again, the basic idea is to perturb the boundary of a solved problem. The major advantage of the method presented is its ability to approximately solve more general problems, that is, problems that are not separable. In addition, we obtain solutions in the form of a partial sum of analytic functions. In general, such solutions are more easy to handle than solutions obtained from characteristics. Finally, the boundary collocation method gives spectral information about the solution. This can help to better understand typical features of hyperbolic BVPs.

4.1. *Solving the two-dimensional Poincaré BVP for a trapezium*

We start by solving the problem considered in § 3. The domain M we begin with is a square with width π (see figure 3). For this geometry, the BVP (3.1) is solved by

$$\psi=\sum_n \psi_n=\sum_n a_n \sin ny \sin nz, \tag{4.1}$$

where the a_n are constant coefficients and $n\in\mathbb{N}$. Maas & Lam (1995) showed that for a square, the a_n are uniquely determined by the Fourier components of the data $f(y)$ along the upper boundary, which is a fundamental interval for the square geometry. This exact relationship is lost if M is changed.

So let us change M by replacing one vertical boundary by a sloping wall. Fundamental intervals corresponding to a square with a sloping sidewall are shown in figure 3 by two bold line segments along the upper boundary. In these intervals, data can be prescribed arbitrarily. This follows from the fact that webs of characteristics

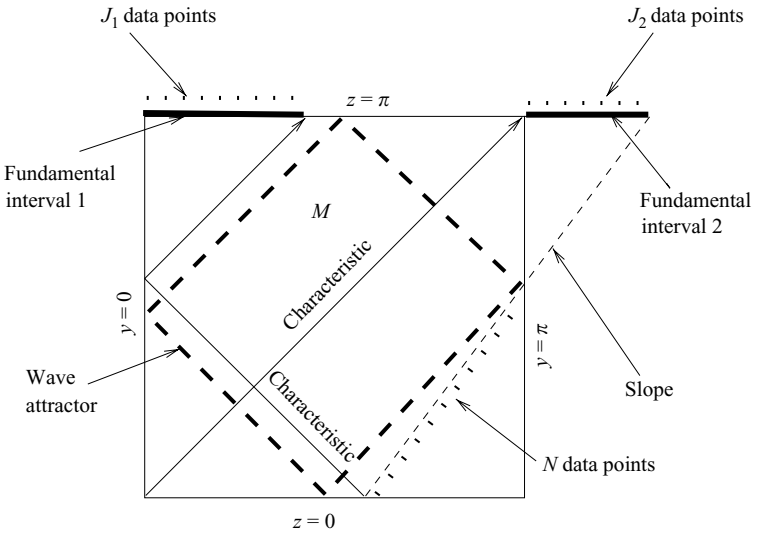

FIGURE 3. The domain M, given by a square with a sloping sidewall (light dashed line). The two fundamental intervals are shown by bold solid lines along the upper boundary. The set of points where data are prescribed are indicated by dotted lines along the fundamental intervals and the lower part of the slope. In total there are $N + J_1 + J_2$ data points. The wave attractor is shown by the bold dashed square.

(i.e. characteristics connected at boundary reflections), launched from fundamental intervals have no reflection point within fundamental intervals. In other words, any characteristic can uniquely be mapped into one of the fundamental intervals. They can be found by following the c^+-characteristic starting at the lower left corner, and the c^--characteristic starting at the bottom of the slope. The latter characteristic shows one reflection at the left boundary.

Obviously, the ψ_n of (4.1) no longer satisfy the boundary conditions along the slope. Nevertheless, we can still write the solution in the form (4.1). In practice, the series has to be truncated, then representing an approximate solution to (3.1)

$$\psi \approx \sum_{n=1}^{\bar{N}} a_n \sin ny \sin nz, \tag{4.2}$$

where $\bar{N} = N + J_1 + J_2$ is the total number of discrete points where data are specified (see dotted lines along the lower part of the slope and above the two fundamental intervals in figure 3). Along the slope it is required that $\psi = 0$; in the two fundamental intervals we prescribe ψ_z. In discrete form we obtain

$$\sum_{n=1}^{\bar{N}} a_n \sin ny_s(i) \sin n(\alpha y_s(i) + c) = 0, \quad i = 1, \ldots, N, \tag{4.3}$$

$$\sum_{n=1}^{\bar{N}} n a_n \sin ny_{f_k}(i) \cos n\pi = b(y_{f_k}(i)), \quad i = 1, \ldots, J_k, \tag{4.4}$$

where $k = 1, 2$, $y_s(i)$ are the grid points along the slope (with $z_s(i) = \alpha y_s(i) + c$, α and c constants), $y_{f_1}(i)$ the grid points along fundamental interval 1, and $y_{f_2}(i)$ the grid points along fundamental interval 2 (see figure 3). The vector $\boldsymbol{b}$ stands for

a prescribed ψ_z at the grid points along the fundamental intervals. In matrix form (4.3)–(4.4) is simply

$$\boldsymbol{A}\cdot\boldsymbol{a} = \boldsymbol{b}, \tag{4.5}$$

where $\boldsymbol{A}$ is a known $\bar{N}\times\bar{N}$ matrix, $\boldsymbol{a}$ is an unknown coefficient vector of length $\bar{N}$, and $\boldsymbol{b}$ a known fundamental data vector of length $\bar{N}$. To find the coefficient vector $\boldsymbol{a}$ we have to invert $\boldsymbol{A}$.

Figure 4 displays an approximate solution of (3.1) for the trapezium by using (4.2) and (4.5). The solution, shown in figure 4(*a*), agrees with the solution presented by Maas *et al.* (1997) (their figure 1B). The location of the square-shaped wave attractor is clearly visible. Note that for this choice of data ψ_z in the fundamental intervals (see the caption of figure 4) the solution is continuous but not differentiable at the location of the wave attractor. Moreover, the solution is antisymmetric with respect to the vertical and horizontal axes, and symmetric with respect to both diagonal axes. We note in passing that a zero level set exists at $y = \pi$. Consequently, the solution shown in figure 4(*a*) is also valid mathematically for a square with length π, although, from a physical viewpoint, an oblique sidewall with focusing reflections is necessary for the existence of a wave attractor. It is important to note that for the discretization given in the caption of figure 4, the condition number κ of $\boldsymbol{A}$ (the ratio of its largest and smallest singular value) is small enough to do a direct numerical inversion of $\boldsymbol{A}$. One must expect to 'lose $\log_{10}\kappa$ digits' when inverting $\boldsymbol{A}$ numerically (Trefethen & Bau 1997, p. 95). MAPLE uses ten digits as the default value for calculations with floating point numbers. Thus, $\kappa < 10^5$ might be acceptable for our purposes.

The spectrum, that is the a_n in (4.2), shown in figure 4(*b*), clearly reflects the antisymmetry of the solution. All coefficients with an odd index are zero which guarantees $\psi = 0$ along $y = z = \pi$, i.e. the antisymmetry of ψ with respect to the diagonal axis of the wave attractor. The first part of the spectrum, determining the largest scales of the solution, shows rather irregular oscillations of large amplitude. For larger wavenumbers ($n > 30$ say), the coefficients are organized as wave packets. They determine the scales resolved close to the wave attractor. By removing single wave packets from the spectrum, we remove part of the fine structure of the wave attractor but do not alter the gross structure of the solution. In figure 4(*c*) we plot a_n^2, $n = 2, 4, 6, \ldots$, together with n^{-2} in a log-log-scale. Obviously, for larger n, the coefficients converge faster to zero than n^{-2}. In spite of this convergence of the sequence of coefficients we anticipate the absence of convergence of the series (4.2) at the attractor, where the streamfunction is not defined (Maas & Lam 1995).

4.2. *Solving the Telegraph BVP for a trapezium*

In this section we consider the Telegraph equation (2.7). The hyperbolic BVP is

$$\psi_{yy} - \psi_{zz} + \alpha^2\psi = 0, \quad \text{with} \quad \psi = 0 \quad \text{at} \quad \partial M, \tag{4.6}$$

where α is constant. Note that the characteristic curves of (4.6) and (3.1) are identical. Nevertheless, (4.6) can neither be solved by the characteristic web method of Maas & Lam (1995), nor the method proposed in § 3, nor by the numerical technique discussed by Swart *et al.* (2007). This is because (4.6) has no formal solution $\psi = f(y+z) - g(y-z)$ that is used in the three methods mentioned. In other words, the benefit that could be derived from characteristic curves to solve (4.6) and (3.1) is different (Harlander & Maas 2006). While we have functions f and g invariant along the characteristic curves for (3.1), such functions do not exist for (4.6), making the BVP mathematically more difficult. However, the boundary collocation method described in § 4.1 is flexible enough to be applied to the BVP (4.6).

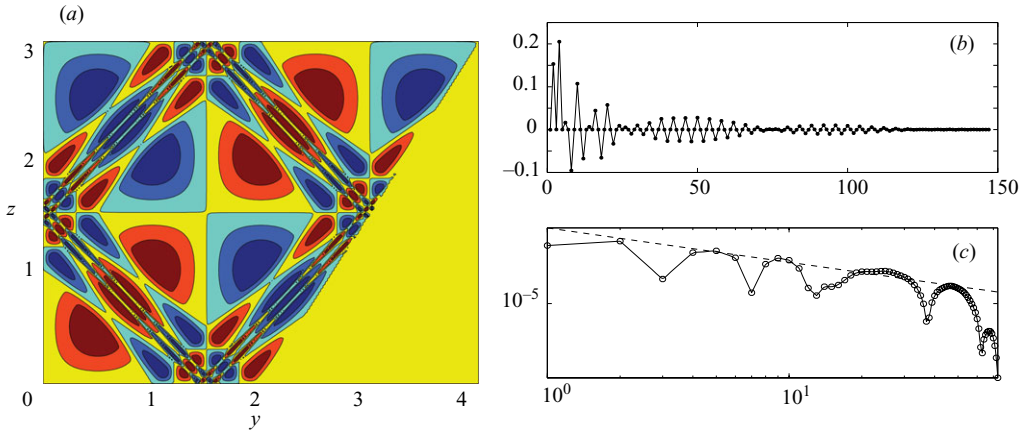

FIGURE 4. Solution of the Poincaré BVP (3.1) for the trapezium: (*a*) streamfunction, (*b*) coefficients a_n, (*c*) square of the even coefficients and n^{-2} (dashed line) in a log-log-frame. For the chosen geometry fundamental intervals one and two are $[0, \pi/3]$ and $[\pi, 4\pi/3]$. We used equally distributed grid points with $N = J_1 = J_2 = 49$ ($\bar{N} = 147$), $y_s(1) = 2.136\ldots$, $y_{f_1}(1) = 0.209\ldots$, and $y_{f_2}(1) = 3.162\ldots$. The sloping wall is given by $z = 3/2y - \pi$, and the data in fundamental intervals one and two are $\psi_z = \sin 3y$ and $\psi_z = -\sin 3y$, respectively. The condition number for $\boldsymbol{A}$ computed with MAPLE is 26921.74.

In a channel with height π solutions of (4.6) are $\psi_n \sim \sin \hat{n} y \sin nz$, where $\hat{n}^2 = n^2 + \alpha^2$. Thus, for a trapezium we can try to find solutions in the form

$$\psi \approx \sum_{n=1}^{\bar{N}} a_n \sin \hat{n} y \sin nz. \tag{4.7}$$

Taking $\alpha = -N^2/(2g) = -0.9$, we proceed analogously to §4.1 to obtain the matrix equation (4.5). We use the same position and number of grid points and the same functions in the fundamental intervals (see the caption of figure 4). The condition number of $\boldsymbol{A}$ is 2598.86, even smaller than in the previous case. Hence, we can directly invert the matrix $\boldsymbol{A}$. For $\alpha \neq 0$, solutions lose the strong symmetry (antisymmetry) present in figure 4(*a*). Moreover, in contrast to the solution of the Poincaré BVP, the solution (4.7) is no longer valid for a square with length π. For the case considered here ($\alpha = -0.9$), the spectrum looks qualitatively similar to the one shown in figure 4(*b*). However, now both even *and* odd modes contribute to the solution of (4.6). Most importantly, the wave attractor is still the dominant feature of the solutions. This is shown in figure 5, where we compare $|\nabla\psi|^2$ from solutions of (3.1) and (4.6) for $\alpha = -0.9$. We see that for the Telegraph equation, which lacks a direct relationship between characteristics and solutions, the web of characteristics still contains valuable information, as was also shown by Rieutord *et al.* (2001) for the Darboux equation. For example the wave attractor still corresponds to the location of singularities and thus to the regions of maximal kinetic energy. In fact, the solution of (4.6) in the neighbourhood of the attractor can be expected to be similar to the solution of (2.8) since the derivatives become very large there and the $\alpha^2\psi$-term can thus be neglected.

4.3. *Solving the Tricomi BVP for a trapezium*

Let us finally consider solutions of the Tricomi BVP

$$\psi_{yy} + y\psi_{zz} = 0, \quad \text{with} \quad \psi = 0 \quad \text{at} \quad \partial M. \tag{4.8}$$

Classically, the Tricomi BVP is given by a boundary curve in the elliptic domain (where $y > 0$) that intersects with the turning curve $y = 0$ at A and B, say. The

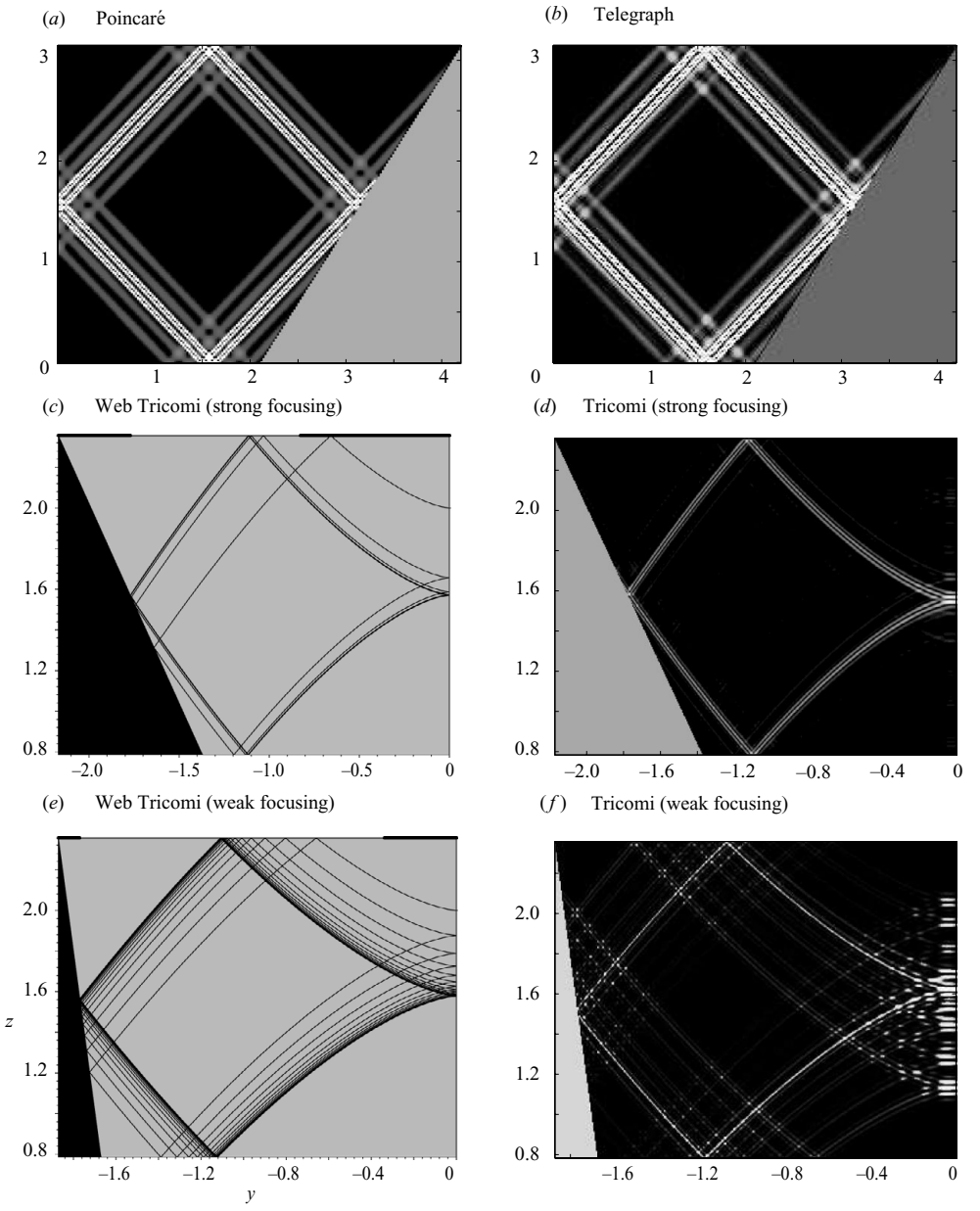

FIGURE 5. $|\nabla\psi|^2$ for (*a*) the two-dimensional Poincaré BVP (3.1), (*b*) the Telegraph BVP (4.6) with $\alpha = -0.9$, and (*d*, *f*) the Tricomi BVP (4.8) for two different slopes. In (*c*) and (*e*) the characteristic webs are shown. Owing to the smaller slope of the left boundary, the characteristics of (*c*) converge faster towards the wave attractor than in (*e*). The two fundamental intervals are shown by bold line segments along the upper boundary in (*c*) and (*e*).

'boundaries' in the hyperbolic domain (where $y < 0$) are given by two characteristics starting at A and B, respectively, and intersecting at a point C in the hyperbolic domain. Dirichlet data are prescribed along the boundary in the elliptic region, and along a certain part of the two characteristics in the hyperbolic region. The goal is to

find regular solutions over the area enclosed by these 'boundaries' (Manwell 1979). In contrast, here we try to solve (4.8) for a boundary geometry that appears to be more useful in the GFD context: M is considered to be a semi-infinite domain, bounded by two lines where z is constant, and a lateral, sloping boundary that closes the domain in the negative y-direction. To the right, the hyperbolic region is 'bounded' by the turning curve $y = 0$ (see figure 5c–f). Nevertheless, the series solution discussed below will also be valid for the elliptic region $y > 0$. As in the previous examples, for this geometry we expect to find solutions with sharp internal boundary layers. It should be noted that like the Telegraph equation, the Tricomi equation does not have a formal solution such as $\psi = f(\zeta) + g(\eta)$, where ζ and η are the characteristic coordinates. Moreover, the characteristics of (4.8) differ from the characteristics of (3.1) and (4.6) (Myint-U 1987, pp. 30–34).

In a strip $y \in \mathbb{R}$, $z \in [\pi/4, 3\pi/4]$ with boundary condition $\psi = 0$ at $z = \pi/4, 3\pi/4$, and $\psi \to 0$ for $y \to \infty$, solutions of (4.8) are $\psi_n \sim \mathrm{Ai}((2n)^{2/3}y)\sin(2n(z+\pi/4))$. Thus, for a geometry like the one shown in figure 5(c–f), we can try to find solutions in the form

$$\psi \approx \sum_{n=1}^{\bar{N}} a_n \mathrm{Ai}((2n)^{2/3}y)\sin(2n(z+\pi/4)), \quad n = 1, 2, 3, \ldots. \tag{4.9}$$

To obtain a simple wave attractor we tilt the left-hand sidewall by two different slopes: $z(y) = -1.963y - 1.906$ causing a fast focusing towards the attractor, and $z(y) = -7.853y - 12.336$, causing a slow focusing (see characteristic webs in figure 5(c,e). For the less steep slope, fundamental intervals one and two are $[y_b - 0.4, y_b]$ and $[-0.8267\ldots, 0]$, respectively, where $y_b = -(3\pi/4)^{2/3}$. For the steep slope, the intervals are $[y_b - 0.1, y_b]$ and $[-0.3382\ldots, 0]$. Then we proceed analogously to § 4.1 to obtain the matrix equation (4.5). In contrast to the previous examples we have to require $\psi = 0$ along the whole slope since ψ now lacks symmetry.

For the Tricomi BVP, the condition number of $\boldsymbol{A}$ is in general much larger than for (3.1) and (4.6). This means that solutions depend more strongly on the number and distribution of the collocation points. For the two choices given above the condition number is $7.00\ldots 10^7$ (fast focusing) and $1.28\ldots 10^{12}$ (slow focusing), and $\boldsymbol{A}$ is said to be ill-conditioned. For ill-conditioned matrices it is not straightforward to do the inversion numerically to solve (4.5). However, the inverse of $\boldsymbol{A}$ can be estimated by employing a technique related to the Moore–Penrose generalized inverse (Moore 1920; Penrose 1955; Aster, Borchers & Thurber 2005). Using singular value decomposition (SVD) we can write the inverse of $\boldsymbol{A}$ as

$$\boldsymbol{A}^{-1} = \boldsymbol{V} \cdot \boldsymbol{W}^{-1} \cdot \boldsymbol{U}^T, \tag{4.10}$$

where $\boldsymbol{U}^T$ is the transpose of the left, and $\boldsymbol{V}$ is the right singular vector of $\boldsymbol{A}$. $\boldsymbol{W}^{-1}$ is diagonal with the elements $1/w_j$, where w_j is the jth singular value of $\boldsymbol{A}$. To estimate the optimal $\boldsymbol{a} = \boldsymbol{A}^{-1} \cdot \boldsymbol{b}$ (in a least-square sense) we have to replace large $1/w_j$-values by zeros and then compute $\boldsymbol{A}^{-1}$ by (4.10) (Press *et al.* 1986). One option for selecting a 'good' solution (Aster *et al.* 2005) is to compute $\epsilon = || \boldsymbol{A} \cdot \tilde{\boldsymbol{a}}_k - \boldsymbol{b} ||_2$ (where $\tilde{\boldsymbol{a}}_k$ stands for $\boldsymbol{a}$ when k reciprocal singular values have been replaced by zeros to compute $\boldsymbol{A}^{-1} \cdot \boldsymbol{b}$) and then use that k that gives a minimum ϵ.

Figure 5(d,f) shows $|\nabla\psi|^2$ for $\bar{N} = N + J_1 + J_2 = 53 + 26 + 16 = 95$ and for $\bar{N} = N + J_1 + J_2 = 39 + 19 + 19 = 77$ by using $k = 4$. We use the same data in the fundamental intervals as in the previous examples. The collocation points are equally distributed with $y_s(1) = -2.155\ldots$, $y_{f_1}(1) = y_s(1)$, and $y_{f_2}(1) = -0.776\ldots$ for the case with the less steep slope, and $y_s(1) = -1.865\ldots$, $y_{f_1}(1) = y_s(1)$, and $y_{f_2}(1) = -0.321\ldots$

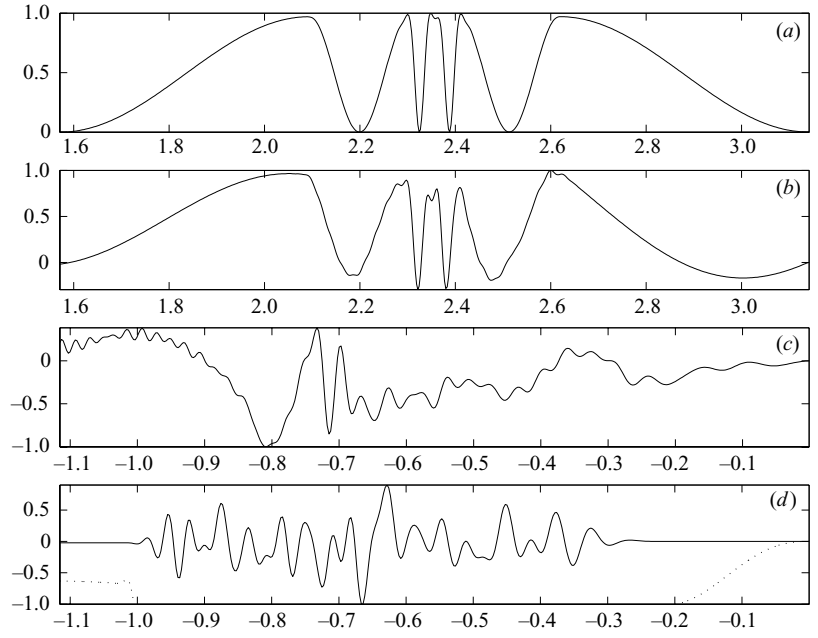

FIGURE 6. Streamfunction ψ for (a) the Poincaré, (b) the Telegraph, and (c) the Tricomi BVP with a strong and (d) a weak focusing. The streamfunction is taken along a characteristic starting at the upper right corner of figures 5(a), 5(b), 5(d), and 5(f) respectively, and ending at $z = \pi/2$. The dotted lines in (d) show the solution when enlarged by a factor $7.28\,10^3$ (right part) and by a factor 29.54 (left part).

for the other case with the steep slope. As in the previous examples, we find internal boundary layers with large streamfunction gradients. Figure 5(c, e) shows webs of characteristics and the wave attractor for the Tricomi BVP. Note that the wave attractor is identical for both slopes. Clearly, this wave attractor agrees well with the position of the strongest internal boundary layers for both cases considered. However, figure 5(f) shows more 'secondary' shear layers than figure 5(d). The layers seem to converge towards the wave attractor, as is implied by the characteristic web shown in figure 5(e). This pattern is reminiscent of solutions recently presented by Rieutord & Valdettaro (1997) (their figure 4) and Ogilvie & Lin (2004) (their figure 11) for the geometry of a spherical shell. Moreover, when focusing is weak, the streamfunction of the Tricomi BVP becomes large at the internal boundary layer. In other words, the solution of the Tricomi BVP is more localized when characteristics converge slowly towards the wave attractor.

This is evident in figure 6, where we plot the streamfunction corresponding to figures 5(a), 5(b), 5(d), and 5(f) along a characteristic that starts at the upper right corner and ends at $z = \pi/2$. Whereas the streamfunction amplitude of the Poincaré, the Telegraph, and the strongly focusing Tricomi BVP remains mainly constant, it doubles at the intersection of the characteristic with the wave attractor for the Tricomi BVP with weak focusing. The exact position of this intersection is given by two characteristics, one sloping downward and starting at $(y, z) = (0, 3\pi/4)$, the other one sloping upward and starting at $(y, z) = (0, 3\pi/8)$. The latter corresponds to the upper right branch of the attractor, shown in figure 5(c, e). The two characteristics intersect at $(y, z) = ((-3\pi/16)^{2/3}, 5\pi/8) \approx (-0.70, 1.96)$; for the case with strong

focusing (figures 5*d*, 6*c*), the maximum of $|\nabla\psi|^2$ can be found at this location. For the other case, the maximum is at about $(-0.67, 1.98)$ (see figures 5*f*, 6*d*). Note that the streamfunction shows a maximum where the wave attractor touches the turning curve $y = 0$ (see figure 5*d*, *f*). There the magnitude of the streamfunction is 3.37 (1.73) times larger than the peak value of $|\psi|$ in figure 6(*c*) (figure 6(*d*)). Note further that the solutions used to plot figure 5(*d*, *f*) are also valid for $y > 0$.

In summary we can conclude that for the Tricomi BVP as well, where we do not have a direct relationship between characteristics and solutions, the web of characteristics can still be used to predict the position of singularities, i.e. the region of maximal kinetic energy (Dintrans *et al.* 1999).

5. Conclusion

Hyperbolic BVPs are difficult to solve since they form mathematically ill-posed problems. A typical feature of such problems is the occurrence of internal shear layers. Energy is strongly localized and no general solution technique is available for these kind of problems. The purpose of the present paper was to add two alternative techniques to the methods already existing.

One technique solves the two-dimensional Poincaré equation by iteratively adjusting the boundary from a non-focusing geometry, where characteristics undergo specular reflections, to a final geometry with focusing reflections. It was shown that the convergence rate of the method depends on the strength of focusing. The new method appears to be faster than the method by Maas & Lam (1995) since characteristics do not have to be traced into fundamental intervals. In fact, fundamental intervals are not needed at all. We considered the rather simple geometry of a rectangle with a sloping part at the bottom. However, it is straightforward to find solutions for more complicated geometries: after having constructed a solution for a boundary 'perturbation' as shown e.g. by the dashed lines in figure 1, a second (or third, etc.) similar local 'perturbation' could be added and a corresponding solution could be obtained iteratively.

The other method proposed is a boundary collocation method. The idea is to superpose smooth solutions (corresponding to a non-focusing boundary geometry) such that, at a set of collocation points along the 'perturbed' part of the boundary and along the fundamental intervals, the solution fulfils the boundary conditions. This gives a discrete linear inverse problem finding unknown coefficients from a linear system of algebraic equations. The advantage of this numerical technique is that it can be applied not only to the two dimensional Poincaré BVP (3.1), but also to more general problems like the Telegraph BVP (4.6) or the Tricomi BVP (4.8), both playing an important role in geophysical fluid dynamics. We first verified the boundary collocation technique by computing the solution for the two-dimensional Poincaré equation in a trapezoidal domain, a problem already solved by Maas *et al.* (1997). Next we solved the Telegraph equation for the same boundary geometry. The solution loses its symmetry. However, we found an internal shear layer at the same position as for the Poincaré problem. For the Tricomi BVP we realized that the matrix that has to be inverted is ill-conditioned, i.e. the ratio of the largest and the smallest singular value of the matrix is large. In this case solutions of the inverse problem are not stable in the sense that they strongly depend on the number and distribution of collocation points; the matrix cannot be inverted numerically without using a regularization technique. To find the solution shown in figure 5(*d*) we computed the generalized inverse and estimated the optimal solution by minimizing the error with

respect to the L_2-norm. This technique is known as Tikhonov regularization (Aster *et al.* 2005).

In agreement with the solutions of the Poincaré and Telegraph BVPs, energy is localized at the wave attractor, that is the limit cycle of the web of characteristics shown in figure 5(*c*). However, in contrast to the other two BVPs, the streamfunction itself is strongly localized for the Tricomi problem: the maximum is located where the wave attractor reflects from the turning curve marking the boundary between the hyperbolic and the elliptic model domain. Such a local maximum can be seen as a strong point source at the boundary of the elliptic region. Thus focusing in the hyperbolic region of a mixed BVP might lead to a deep penetration of energy into the elliptic domain. This could have implications for telecommunications through the oceans or the atmosphere, where equatorial and extratropical waveguides are separated by elliptic regions. Owing to focusing in the equatorial hyperbolic region there might be an effective 'tunnelling' of low-frequency waves through the elliptic domain, triggering Rossby waves in the extratropics. Further work is required to understand better this possibility of tropical–extratropical interaction.

In Appendix B we roughly estimate time mean dissipation rates $\bar{D}$ for the two-dimensional Poincaré BVP when Rayleigh friction or viscous damping is switched on at $t = 0$. For this purpose we assume that the time scale of the damping is much larger than the time scale of the oscillations. By using the series solution (4.1) we obtain compact expressions, for Rayleigh friction as well as viscous damping. In future work we hope to find analytic expressions for the coefficients. Moreover, we will try to include forcing in order to compare the results with recent findings on the non-zero asymptotic dissipation rate of tidal disturbances (Ogilvie 2005).

It should be noted that we did not solve a general hyperbolic initial BVP. For certain elliptic problems (e.g. the Helmholtz equation with Dirichlet boundary conditions), solutions for arbitrary initial data can be constructed by superposing eigenfunctions, forming a complete set of orthogonal functions. For hyperbolic BVPs, spectra are usually dense and solutions constructed for different frequencies are usually not orthogonal for any choice of data in the fundamental intervals. For some hyperbolic BVPs it is known that only singular solutions exist. So it remains mathematically challenging to find the time evolution of such problems starting from an arbitrary (smooth) initial field. Nevertheless, the development of reliable techniques to solve hyperbolic BVP is certainly indispensable to tackle hyperbolic initial BVPs in the future.

We thank Theo Gerkema and Sjef Zimmerman for heplful discussions and the anonymous referees for many constructive suggestions improving the paper. U.H. was supported by the Netherlands Organization for Scientific Research (N.W.O.) under grant 813.03.004 (ALW3PJ/03-23).

Appendix A. The Riemann method

At a given point $P = (\eta_0, \zeta_0)$ the solution of a linear second-order hyperbolic equation

$$\psi_{\eta\zeta} + a\psi_\eta + b\psi_\zeta + c\psi = 0 \tag{A 1}$$

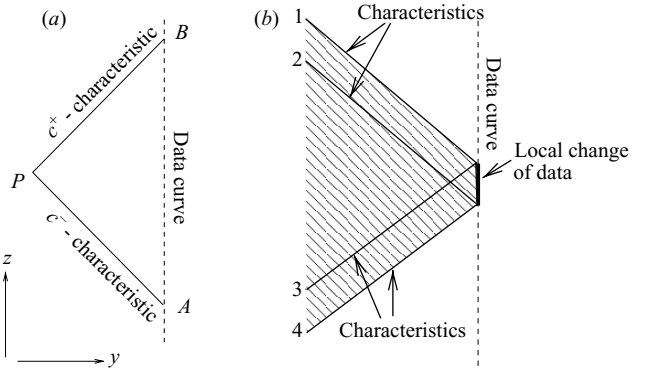

FIGURE 7. (*a*) Definition of P, A, and B. (*b*) A local change of ψ along the data curve where $\psi_y = 0$ changes the solution of the Poincaré problem between the characteristics 1,2 and 3,4. For more general problems the solution will be changed in the hatched area.

can be written as (Myint-U 1987, pp. 76–83),

$$\psi_P = \frac{1}{2}((\psi R)\,|_A + (\psi R)\,|_B) - \int_A^B \psi R\,(a\mathrm{d}\eta - b\mathrm{d}\zeta)$$
$$-\frac{1}{2}\int_A^B \psi(R_\zeta \mathrm{d}\zeta - R_\eta \mathrm{d}\eta) + \frac{1}{2}\int_A^B R(\psi_\zeta \mathrm{d}\zeta - \psi_\eta \mathrm{d}\eta), \qquad (A\,2)$$

where (η, ζ) are the characteristic coordinates and $R = R(P, \eta, \zeta)$ denotes the Riemann function, and A, B give the position of intersection of the c^-- and c^+-characteristics with the curve on which data are prescribed (see figure 7). To obtain straight characteristics with slopes ± 1 we introduce $(y, z) = (\zeta - \eta, \zeta + \eta)$. In these coordinates (A 2) becomes

$$\psi_P = \frac{1}{2}\left((\psi R)\,|_A + (\psi R)\,|_B\right) - \frac{1}{2}\int_A^B \psi R\,((a-b)\mathrm{d}z - (a+b)\mathrm{d}y)$$
$$-\frac{1}{2}\int_A^B \psi\left(R_z \mathrm{d}y + R_y \mathrm{d}z\right) + \frac{1}{2}\int_A^B R\left(\psi_z \mathrm{d}y + \psi_y \mathrm{d}z\right). \qquad (A\,3)$$

For the Poincaré equation, $a = b = c = 0$ and $R = 1$. If we prescribe data $\psi = f(z)$, $\psi_y = 0$, along a curve $y =$ constant, then only the first two terms on the right-hand side of (A 3) are non-zero. Note that for the Telegraph and Tricomi equations as well, the Riemann functions are known (Myint-U 1987; Manwell 1979). However, for a closed domain, only the Poincaré equation can be solved using (A 3). The reason is that: (i) the inverse problem of finding ψ-data from the condition $\psi_P = 0$ along a curve l is complicated when $a, b \neq 0$ and $R = R(y, z)$; and (ii) changing ψ locally along the data curve while keeping $\psi_y = 0$ gives a local response for the Poincaré BVP but a global response for more general problems that have non-vanishing second and third terms in (A 3) (see figure 7*b*).

Appendix B. Dissipation

With the spectra a_n to hand we can ask how much energy will be dissipated in a given time when we switch on a dissipative term.

Let us write a prototypical vorticity equation as

$$\frac{\partial^2}{\partial t^2}\nabla^2\psi - F = -\nu\frac{\partial}{\partial t}R, \tag{B 1}$$

where F denotes other linear terms in ψ, and R is a damping term, given as $R = (-1)^m\nabla^{2m}\nabla^2\psi$. The constant ν is the kinematic viscosity coefficient, and $m = 0, 1, 2, \ldots$, determines the damping characteristic. (For $m = 0$ damping is due to the so called Rayleigh friction; for $m = 1$ damping is caused by momentum diffusion. Models with $m > 1$ are called hyper-diffusive.) We assume that $\psi = \psi(\tilde{t}, T, y, z)$, where $\tilde{t} = t$ is the fast time scale of the oscillation, and $T = \nu t/2$ is the slow time scale of the damping. Then the time derivative can be written as $\partial/\partial t = \partial/\partial\tilde{t} + (\nu/2)\partial/\partial T$. If the solution of (B 1) is written as $\psi = \sum_n \hat{a}_n(T)\psi_n(y, z)\exp(\mathrm{i}\tilde{t})$, we find to order ν^0 and order ν^1

$$\nu^0: \quad \frac{\partial^2}{\partial\tilde{t}^2}\nabla^2\psi - F = 0, \tag{B 2}$$

$$\nu^1: \quad \frac{\partial}{\partial\tilde{t}}\frac{\partial}{\partial T}\nabla^2\psi + \frac{\partial}{\partial\tilde{t}}R = 0. \tag{B 3}$$

From (B 2) we see that the ψ_n are simply the inviscid modes, corresponding for example to (3.1) or (4.6). Finally, from (B 3) we obtain $\hat{a}_n = a_n\exp(-\nu k^{2m}t)$, where k is the total wavenumber and the a_n are the coefficients of the inviscid problem, determined via the boundary conditions.

With the spectrum $\hat{a}_n$ to hand, we can now estimate the dissipation rate

$$D(t) = \int_M \nu \mid \nabla^{m+1}\psi \mid^2 \mathrm{d}y\,\mathrm{d}z, \quad m = 0, 1, \tag{B 4}$$

for non-conservative hyperbolic BVPs. Note that in figure 5(a, b, d, f) we plotted the integrand of (B 4) for $m = 0$; that is the plots show the spatial distribution of the dissipation rate. Clearly, dissipation will be large at the wave attractor and its neighbourhood.

In the following we estimate a mean dissipation rate for the two-dimensional Poincaré BVP (2.8). To perform the spatial integration we can make use of the fact that the attractor solution is valid not only over the trapezium, but also over the square $y \in [0, \pi]$, $z \in [0, \pi]$ (see figure 4a). In other words, we first rotate the triangle given by $(y, z) = (\pi, \pi/2), (\pi, \pi), (4\pi/3, \pi)$ clockwise by π and then integrate over the square with length π. This integration is equal to the integration over the trapezium. We find

$$D(t) = \begin{cases} \nu\frac{1}{2}\pi^2\sum_n n^2\hat{a}_n^2 & \text{if } m = 0, \\ \nu\pi^2\sum_n n^4\hat{a}_n^2 & \text{if } m = 1. \end{cases} \tag{B 5}$$

Finally, the time mean dissipation rate results from integrating (B 5) over time

$$\bar{D} = \int D(t)\,\mathrm{d}t = -\frac{\pi^2}{4}\sum_n \mathrm{e}^{-s(n)}n^2a_n^2, \tag{B 6}$$

where

$$s(n) = \begin{cases} 2\nu t & \text{if } m = 0, \\ 4\nu n^2 t & \text{if } m = 1. \end{cases} \tag{B 7}$$

Considering the time period from $t = 0$ to $t = \bar{t}$ we find that, for a bounded $\bar{D}$, the coefficients a_n^2 have to converge faster than n^{-2}. This is the case for the

truncated solution, as can be seen in figure 4(*c*). However, for a mathematically sound understanding of the convergence, an analytic expression for the coefficients is needed.

By specifying $\bar{t} = 1/(2\nu)$, we can expect from (B 6) that, because of the fast decrease of $\exp(-2n^2)$ with increasing n, the ratio between the viscous and the Rayleigh friction damping rate will be about $e/(e-1) \approx 1.582$. Using the coefficients shown in figure 4(*b*), we indeed find a ratio of 1.584. Hence, when averaged over a period as long as $1/(2\nu)$, Rayleigh damping is almost as effective as viscosity. Note that for the solution shown in figure 4(*a*), only the coefficients with even n are non-zero.

REFERENCES

Aster, R. C., Borchers, B. & Thurber, C. H. 2005 *Parameter Estimation and Inverse Problems*. Elsevier.

Brown, S. N. & Stewartson, K. 1976 Asymptotic methods in the theory of rotating fluids. In *Asymptotic Methods and Singular Perturbations* (ed. R. E. O'Malley), pp. 1–21. SIAM-AMS Proceedings, vol. 10, American Mathematical Society.

Bryan, G. H. 1889 The waves on a rotating liquid spheroid of finite ellipticity. *Phil. Trans. R. Soc. Lond.* **180**, 187–219.

Dintrans, B., Rieutord, M. & Valdettaro, L. 1999 Gravito-inertial waves in a rotating stratified sphere or spherical shell. *J. Fluid Mech.* **398**, 271–297.

Friedlander, S. 1982 Turning surface behaviour for internal waves subject to general gravitational field. *Geophys. Astrophys. Fluid Dyn.* **21**, 189–200.

Friedlander, S. & Siegmann, W. L. 1982 Internal waves in a rotating stratified fluid in an arbitrary gravitational field. *Geophys. Astrophys. Fluid Dyn.* **19**, 267–291.

Harlander, U. & Maas, L. R. M. 2006 Characteristics and energy rays of equatorially trapped, zonally symmetric internal waves. *Meteorologische Z.* **15**, 439–450.

Hollerbach, R. & Kerswell, R. R. 1995 Oscillatory internal shear layers in rotating and precessing flows. *J. Fluid Mech.* **298**, 327–339.

Kelvin, Lord 1880 Vibrations of a columnar vortex. *Phil. Mag.* **10**, 155–168.

Maas, L. R. M. 2005 Wave attractors: linear yet nonlinear. *Int. J. Bifurcation Chaos,* **15**, 2757–2782.

Maas, L. R. M., Benielli, D., Sommeria, J. & Lam, F.-P. A. 1997 Observation of an internal wave attractor in a confined, stable stratified fluid. *Nature* **388**, 557–561.

Maas, L. R. M. & Harlander, U. 2007 Equatorial wave attractors and inertial oscillations. *J. Fluid Mech.* **570**, 47–67.

Maas, L. R. M. & Lam, F.-P. A. 1995 Geometric focusing of internal waves. *J. Fluid Mech.* **300**, 1–41.

Manwell, A. R. 1979 *The Tricomi Equation with Applications to the Theory of Plane Transonic Flow*. Pitman.

Moore, E. H. 1920 On the reciprocal of the general algebraic matrix. *Bull. Am. Math. Soc.* **26**, 394–395.

Morse, P. M. & Feshbach, H. 1953 *Methods of Theoretical Physics, Vol. I & II*. McGraw-Hill.

Myint-U, T. 1987 *Partial Differential Equations for Scientists and Engineers,* 3rd End. North Holland.

Ogilvie, G. I. 2005 Wave attractors and the asymptotic dissipation rate of tidal disturbances. *J. Fluid Mech.* **543**, 19–44.

Ogilvie, G. I. & Lin, D. N. C. 2004 Tidal dissipation in rotating giant planets. *Astrophys. J.* **610**, 477–509.

Payne, L. E. 1975 *Improperly Posed Problems in Partial Differential Equations*. SIAM.

Penrose, R. 1955 A generalized inverse for matrices. *Proce. Camb. Phil. Soc.* **51**, 406–413.

Press, W. H., Flannery, B. P., Teukolsky, S. A. & Vetterling, W. T. 1986 *Numerical Recipes: The Art of Scientific Computing*. Cambridge University Press.

Rieutord, M., Georgeot, B. & Valdettaro, L. 2000 Wave attractors in rotating fluids: a paradigm for ill-posed Cauchy problems. *Phys. Rev. Lett.* **85**, 4277–4280.

Rieutord, M., Georgeot, B. & Valdettaro, L. 2001 Inertial waves in a rotating spherical shell: attractors and asymptotic spectrum. *J. Fluid Mech.* **435**, 103–144.

Rieutord, M. & Valdettaro, L. 1997 Inertial waves in a rotating spherical shell. *J. Fluid Mech.* **341**, 77–99.

Slavyanov, S. Y. & Lay, W. 2000 *Special Functions: A Unified Theory based on Singularities*. Oxford University Press.

Stewartson, K. & Rickard, J. A. 1969 Pathological oscillations of a rotating fluid. *J. Fluid Mech.* **5**, 577–592.

Swart, A., Sleijpen, G. L. G., Maas, L. R. M. & Brandts, J. 2007 Numerical solution of the two-dimensional Poincaré equation. *J. Comput. Appl. Math.* **200**, 317–341.

Trefethen, L. N. & Bau, D. 1997 *Numerical Linear Algebra*. SIAM.